Article

Cell Reports

Glutathione Transferase Omega-1 Regulates NLRP3 Inflammasome Activation through NEK7 Deglutathionylation

Graphical Abstract

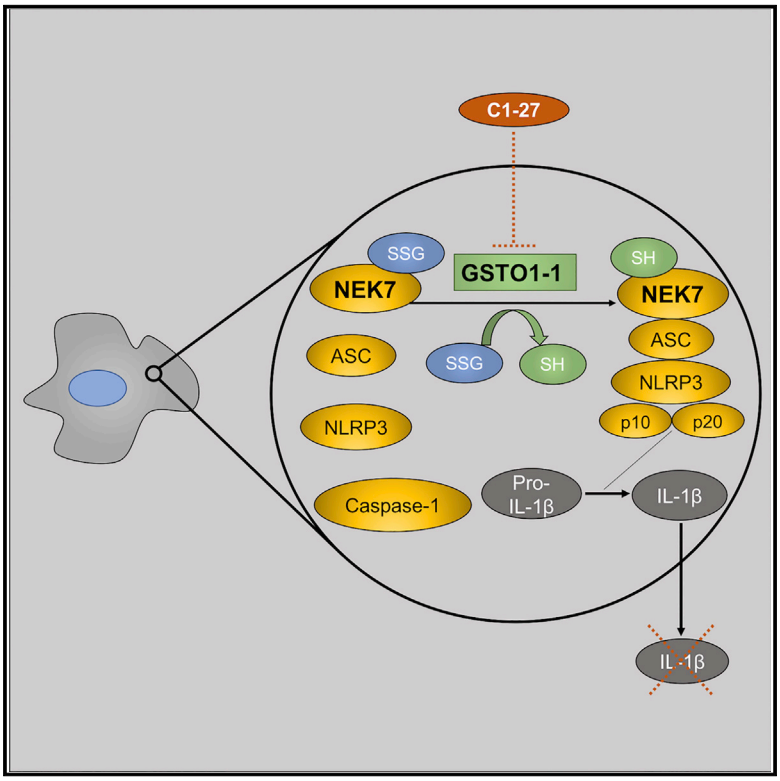

Authors

Mark M. Hughes, Alexander Hooftman, Stefano Angiari, ..., Jonathan B. Baell, Philip G. Board, Luke A.J. O'Neill

Correspondence

laoneill@tcd.ie

In Brief

NLRP3 inflammasome activation contributes to chronic inflammation associated with autoinflammatory disease, yet understanding of NLRP3 inflammasome regulation is incomplete. Hughes et al. show that the deglutathionylating enzyme GSTO1-1 promotes NLRP3 inflammasome activation through deglutathionylation of NEK7. Furthermore, the GSTO1-1 inhibitor C1-27 reduces NLRP3 inflammasome activation *in vitro* and *in vivo*.

Highlights

- C1-27, a small molecule inhibitor of GSTO1-1, inhibits NLRP3 inflammasome activation
- GSTO1-1 deglutathionylates NEK7 on cysteine 253 to promote NLRP3 inflammasome activation
- C1-27 is protective *in vivo* in a model of experimental autoimmune encephalomyelitis

Hughes et al., 2019, Cell Reports *29*, 151–161
October 1, 2019
https://doi.org/10.1016/j.celrep.2019.08.072

CellPress

Cell Reports
Article

Glutathione Transferase Omega-1 Regulates NLRP3 Inflammasome Activation through NEK7 Deglutathionylation

Mark M. Hughes,[1,7,11] Alexander Hooftman,[1,11] Stefano Angiari,[1] Padmaja Tummala,[2] Zbigniew Zaslona,[1] Marah C. Runtsch,[1] Anne F. McGettrick,[1] Caroline E. Sutton,[1] Ciana Diskin,[1] Melissa Rooke,[2] Shuhei Takahashi,[10] Srinivasan Sundararaj,[2] Marco G. Casarotto,[2] Jane E. Dahlstrom,[8] Eva M. Palsson-McDermott,[1] Sinead C. Corr,[3] Kingston H.G. Mills,[1] Roger J.S. Preston,[7] Nouri Neamati,[4,5,6] Yiyue Xie,[9] Jonathan B. Baell,[9] Philip G. Board,[2] and Luke A.J. O'Neill[1,12,*]

[1]School of Biochemistry and Immunology, Trinity Biomedical Sciences Institute, Trinity College Dublin, Dublin 2, Ireland
[2]John Curtin School of Medical Research, Australian National University, Canberra, ACT 2601, Australia
[3]Department of Microbiology, Moyne Institute of Preventive Medicine, School of Genetics and Microbiology, Trinity College Dublin, Dublin 2, Ireland
[4]Department of Pharmacology and Pharmaceutical Sciences, School of Pharmacy, University of Southern California, 1985 Zonal Avenue, Los Angeles, CA 90033, USA
[5]Department of Medicinal Chemistry, College of Pharmacy, University of Michigan, 2800 Plymouth Road, Building 520, Room 1363, Ann Arbor, MI 48109, USA
[6]Translational Oncology Program, University of Michigan, 2800 Plymouth Road, Building 520, Room 1363, Ann Arbor, MI 48109, USA
[7]Molecular and Cellular Therapeutics, Royal College of Surgeons in Ireland, Dublin 2, Ireland
[8]ACT Pathology and ANU Medical School, The Canberra Hospital, Canberra, ACT, Australia
[9]Monash Institute of Pharmaceutical Sciences, Monash University, Parkville, VIC 3052, Australia
[10]Department of Human Pathology, Graduate School and Faculty of Medicine, Tokyo Medical and Dental University, Tokyo 113-8510, Japan
[11]These authors contributed equally
[12]Lead Contact
*Correspondence: laoneill@tcd.ie
https://doi.org/10.1016/j.celrep.2019.08.072

SUMMARY

The NLRP3 inflammasome is a cytosolic complex sensing phagocytosed material and various damage-associated molecular patterns, triggering production of the pro-inflammatory cytokines interleukin-1 beta (IL)-1β and IL-18 and promoting pyroptosis. Here, we characterize glutathione transferase omega 1-1 (GSTO1-1), a constitutive deglutathionylating enzyme, as a regulator of the NLRP3 inflammasome. Using a small molecule inhibitor of GSTO1-1 termed C1-27, endogenous GSTO1-1 knockdown, and GSTO1-1$^{-/-}$ mice, we report that GSTO1-1 is involved in NLRP3 inflammasome activation. Mechanistically, GSTO1-1 deglutathionylates cysteine 253 in NIMA related kinase 7 (NEK7) to promote NLRP3 activation. We therefore identify GSTO1-1 as an NLRP3 inflammasome regulator, which has potential as a drug target to limit NLRP3-mediated inflammation.

INTRODUCTION

The NLRP3 inflammasome is an intracellular pattern recognition receptor (PRR) that is activated by phagocytosed particles or agents such as ATP and mitochondrial DNA. Activation drives oligomerization with the adaptor protein apoptosis-associated speck-like protein containing a CARD (ASC), pro-caspase-1 (Martinon et al., 2002), and the recently described inflammasome component NEK7, a serine/threonine kinase that also functions in mitosis (Shi et al., 2016b; He et al., 2016; Yissachar et al., 2006; Sharif et al., 2019). Activation of the NLRP3 inflammasome results in processing of pro-interleukin-1 beta (pro-IL-1β) and pro-IL-18 to mature cytokines and also triggers pyroptosis in macrophages (Fink and Cookson, 2006). These events are highly inflammatory, and as a result NLRP3 is tightly regulated post-translationally. NLRP3 phosphorylation in its pyrin domain (PYD) limits inflammasome assembly (Stutz et al., 2017), as does ubiquitination (Juliana et al., 2012).

Inflammatory insults can trigger oxidative dysfunction, inducing reactive oxygen species (ROS) production to trigger NLRP3 inflammasome activation (Zhou et al., 2011). NEK7 has been recently identified as a ROS-sensing NLRP3 inflammasome component, requiring ROS for its phosphorylation and subsequent interaction with NLRP3 (Shi et al., 2016b; Groß et al., 2016), although the precise mechanism of how ROS affects NEK7 is unknown. Further, chloride intracellular channel (CLIC) family members drive NLRP3 inflammasome activation. CLIC translocation triggers chloride and potassium (K^+) efflux, which promotes NEK7-NLRP3 interaction, events that are also dependent on mitochondrial ROS (Domingo-Fernández et al., 2017; Tang et al., 2017).

Glutathione (GSH) is the major non-protein tripeptide antioxidant present within cells and can modify target cysteines via glutathionylation and alter protein function (Hughes et al., 2017; Ullevig et al., 2016; Zhang et al., 2017). Glutathione

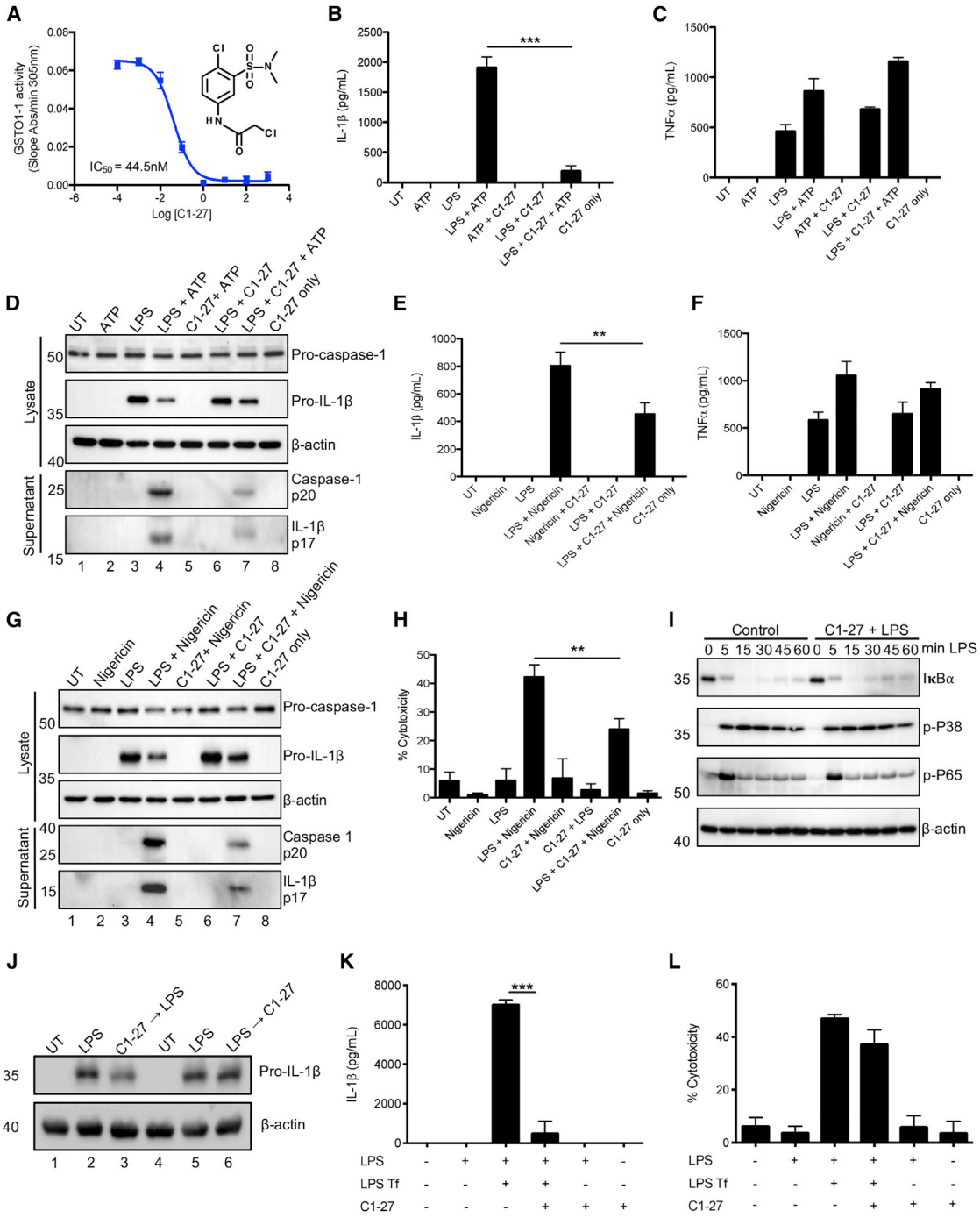

Figure 1. C1-27 Limits NLRP3 Inflammasome Activation

(A) Inhibition of GSTO1-1-catalyzed 4-nitrophenacyl glutathione reduction by C1-27 dose dependently. The structure of C1-27 is displayed (n = 3).

(B and C) ELISA of IL-1β (B) and TNF-α (C) in supernatants from BMDMs primed with 3 h LPS, incubated with 5 μM C1-27 for 45 min, and stimulated with 5 mM ATP for 45 min (n = 3).

(D) Immunoblots corresponding to BMDMs treated as in (B) and (C) (n = 3).

(E and F) ELISA of IL-1β (E) and TNF-α (F) in supernatants from BMDMs primed with LPS, incubated with 5 μM C1-27, and stimulated with 10 μM nigericin (n = 3).

(G) Immunoblot corresponding to BMDMs treated as in (E) and (F) (n = 3).

(H) Pyroptosis of BMDMs treated from (E) and (F) measured by secretion of lactate dehydrogenase (LDH) into the supernatant. % Cytotoxicity was calculated relative to total lysis control of unstimulated cells (n = 3).

(I) Immunoblot of BMDMs pre-treated with 5 μM C1-27 and stimulated with LPS for indicated times (n = 3).

(legend continued on next page)

transferase omega 1-1 (GSTO1-1) is a constitutively active deglutathionylating enzyme and has recently been implicated in inflammatory macrophage activation downstream of TLR4 (Menon et al., 2014, 2017). GSTO1-1 has also been found in a complex with ASC, a key inflammasome component (Coll et al., 2011). We therefore examined a role for GSTO1-1 in NLRP3 activation. We provide evidence for GSTO1-1 as a regulator of the NLRP3 inflammasome and identify NEK7 as a target. NEK7 must undergo deglutathionylation in order to be active. Our findings suggest that the targeting of GSTO1-1 has potential as a strategy to limit inflammation.

RESULTS

The GSTO1-1 Inhibitor C1-27 Limits NLRP3 Inflammasome Activation

To examine a role for GSTO1-1 in the NLRP3 inflammasome, we used a recently described GSTO1-1 inhibitor, termed C1-27 (Ramkumar et al., 2016). ML175, a GSTO1-1 inhibitor that had been used in previous studies, was found to be toxic on macrophages (Figures S1A and S1B). C1-27 potently inhibits GSTO1-1, with a half maximal inhibitory concentration (IC_{50}) of 44.5 nM (Figure 1A). C1-27 dose-dependently blocked NLRP3 inflammasome stimulation when added after lipopolysaccharide (LPS) priming and before ATP stimulation (Figure S1C), and a concentration of 5 μM was selected for future experiments. Following priming with LPS, C1-27 inhibited ATP-stimulated NLRP3 activation, limiting IL-1β release (Figure 1B), with no effect on tumor necrosis factor alpha (TNF-α) secretion (Figure 1C). Mature caspase-1 p20 and mature IL-1β p17 were also significantly reduced by C1-27 (Figure 1D, supernatant panels, compare lane 7 to lane 4). C1-27 treatment of LPS-primed bone-marrow-derived macrophages (BMDMs) also limited IL-1β secretion in response to nigericin stimulation (Figure 1E), with no difference in TNF-α secretion (Figure 1F). Similar to ATP treatment, C1-27 reduced mature caspase-1 p20 and mature IL-1β p17 secretion into the supernatant (Figure 1G, supernatant panels, compare lane 7 to lane 4). In addition, cell death mediated by nigericin-stimulated inflammasome activation was significantly reduced by C1-27 treatment (Figure 1H). Similar to BMDMs, C1-27 significantly inhibited the release of IL-1β from human peripheral blood mononuclear cells (PBMCs) (Figures S1D and S1E). Human PBMCs produce IL-1β upon LPS stimulation alone, but this is increased by addition of nigericin. C1-27 inhibited IL-1β release when added before LPS stimulation (Figure S1D) but also when added between LPS priming and nigericin stimulation (Figure S1E). To assess if C1-27 was affecting TLR4 signaling, we examined the phosphorylation of downstream activation markers of TLR4 action. C1-27 pre-treatment did not limit degradation of IκBα (nuclear factor of kappa light polypeptide gene enhancer in B cells inhibitor, alpha), nor did it limit phosphorylation of p38 and p65 (Figure 1I). We also assessed whether C1-27 treatment prior to or post LPS priming would impact pro-IL-1β production in BMDMs. C1-27 pre-treatment reduced pro-IL-1β production in BMDMs but not post-LPS treatment (Figure 1J). We next assessed if C1-27 could limit non-canonical inflammasome activation via transfected LPS (Kayagaki et al., 2011). C1-27 treatment prior to LPS transfection significantly reduced IL-1β secretion (Figure 1K). C1-27 was unable to limit pyroptosis associated with caspase-11 activation, an event that is NLRP3 independent (Figure 1L), suggesting specificity toward NLRP3. We therefore next examined whether C1-27 would inhibit AIM2 or NLRC4 inflammasome activation. C1-27 pre-treatment prior to poly (dA:dT) transfection was unable to limit IL-1β secretion (Figure S2A). C1-27 did not limit mature caspase-1 p20 or mature IL-1β p17 secretion into the supernatant (Figure S2B, supernatant panels, compare lane 7 to lane 4). We also assessed NLRC4 inflammasome activation. LPS-primed macrophages were pre-treated with C1-27 prior to *Salmonella typhimurium* UK-1 infection. Similar to the AIM2 inflammasome, C1-27 did not reduce IL-1β secretion in response to *S. typhimurium* (Figure S2C). Both mature caspase-1 p20 and mature IL-1β p17 release were also unaffected by C1-27 (Figure S2D, supernatant panels, compare lane 7 to lane 4). GSTO1-1 has previously been identified as a target for cytokine release inhibitory drug (CRID) compounds (Laliberte et al., 2003). A derivative of CRID3, termed MCC950, is a potent NLRP3 inflammasome inhibitor (Coll et al., 2015). Due to the similarities between C1-27 and MCC950, we assessed if MCC950 could inhibit GSTO1-1 enzymatic activity. MCC950 was a poor GSTO1-1 inhibitor, with an IC_{50} of 124.8 μM (Figure S2E). These data suggest that GSTO1-1 can regulate the NLRP3 inflammasome by canonical and non-canonical activators and is unlikely to be the target for MCC950 in the NLRP3 inflammasome.

C1-27 Reduces ASC Speck Formation

Activation of the NLRP3 inflammasome results in oligomerization of ASC through its PYD to form ASC specks (Lu et al., 2014), an event upstream of caspase-1 activation. To gain insight into the regulation of the NLRP3 inflammasome by GSTO1-1, we assessed if C1-27 could reduce the formation of ASC oligomers. Using disuccinimidyl suberate crosslinking, LPS and ATP stimulation of BMDMs induced oligomerization of ASC, detected in the Triton X-100 insoluble fraction by immunoblotting. Treatment with C1-27 prior to ATP stimulation reduced ASC oligomerization (Figure 2A, Triton-insoluble panel, compare lane 4 to lane 3). Monomeric ASC was also examined in the Triton X-100 soluble fraction. In response to LPS and ATP, ASC monomers were significantly depleted compared to C1-27 treatment (Figure 2A, Triton-soluble panel, lane 3). ASC monomers were more prominent in the C1-27-treated cells (Figure 2A, Triton-soluble panel, lane 4). ASC oligomerization was also assessed by confocal microscopy, whereby ASC oligomers form punctate specks (Masumoto et al., 1999; Sahillioglu et al., 2014). BMDMs stimulated with LPS and ATP showed increased presence of ASC specks (Figure 2B, third panel). Pre-treatment

(J) Immunoblot of BMDMs treated with 5 μM C1-27 for 1 h before (lanes 1–3) or after (lanes 4–6) 4 h LPS treatment (lanes 1–3) (n = 3).
(K and L) BMDMs were primed with 100 ng/mL LPS for 4 h, treated with 5 μM C1-27 for 2 h, and transfected with 1 μg/mL LPS for 16 h. Supernatant was harvested for IL-1β ELISA (K) or LDH release (L) (n = 3).
Data are mean ± SEM; p values calculated using one-way ANOVA with Sidak's multiple comparisons test (**p < 0.01, ***p < 0.001).

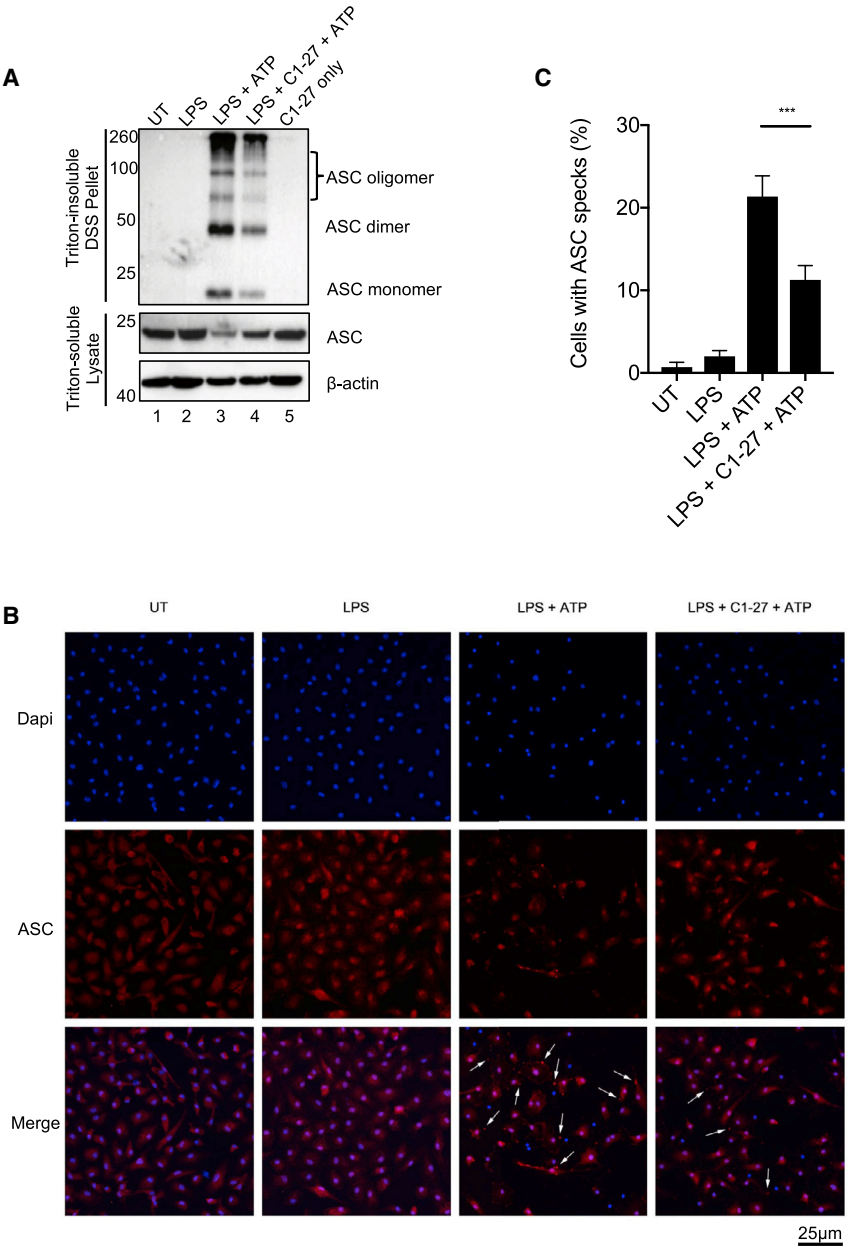

Figure 2. C1-27 Reduces ASC Speck Formation

(A) BMDMs were primed with LPS for 3 h, incubated with 5 μM C1-27 for 45 min, and stimulated with 5 mM ATP for 45 min. Cells were lysed in lysis buffer containing Triton X-100. Triton X-100-insoluble fraction was crosslinked using disuccinimidyl suberate. Both the soluble and insoluble fractions were analyzed by immunoblot for ASC expression (n = 3).

(B) Confocal microscopy analysis of ASC speck formation in BMDMs. BMDMs were plated on sterile 12-mm cover glasses and stimulated as (A). Following stimulation they were stained with rabbit anti-ASC antibody and anti-rabbit Alexa Fluor 647 and ProLong Gold antifade reagent with DAPI. Images were acquired ×20 magnification (n = 4).

(C) For quantification of ASC speck-positive cells, a minimum of 11 random regions of interest for each experimental condition across four independent experiments were imaged and the number of ASC speck-positive cells were counted (n = 4).

Data are mean ± SEM; p values calculated using one-way ANOVA with Sidak's multiple comparisons test (***$p < 0.001$).

with C1-27 reduced the level of ASC speck formation (Figure 2B, fourth panel). These changes were quantified, demonstrating that C1-27 significantly reduced the percentage of ASC speck-positive cells (Figure 2C), thereby suggesting that GSTO1-1 is involved in NLRP3 inflammasome assembly.

C1-27 Is Active *In Vivo* and Reduces Inflammasome Activation Associated with DSS-Induced Colitis and Experimental Autoimmune Encephalomyelitis

Mice deficient in NLRP3, caspase-1, and ASC have been found to be highly sensitive to distal colon inflammation in the dextran sodium sulfate (DSS) model of inflammatory bowel disease (Allen et al., 2010; Zaki et al., 2010). It was considered that the lack of IL-18 processing led to a breakdown in the intestinal barrier, resulting in the escape of bacteria and an increase in inflammation. We have previously found that GSTO1-1-deficient mice are also susceptible to inflammation in the DSS model (Menon et al., 2017). We therefore next tested C1-27 in the DSS model and found that C1-27 recapitulates the decreased cytokine release observed in GSTO1-1$^{-/-}$ mice. At day 8, GSTO1-1$^{-/-}$ mice or mice treated with C1-27 showed a significant reduction in the levels of IL-18 in serum and in the supernatant obtained from colon slices cultured for 24 h (Figures 3A and 3B). Similar results were obtained for IL-1β in colon culture supernatants (Figure 3C), but the levels of IL-1β in serum were low and not reliably detected in this study (<10 pg/mL; data not shown). To determine if 8-day treatment with C1-27 had a measurable impact on GSTO1-1 activity, we determined the level of GSTO1-1 activity in the liver with the specific substrate 4-nitrophenacyl glutathione (Board et al., 2008) (Figure 3D). GSTO1-1 activity was absent from GSTO1-1$^{-/-}$ mice and was significantly diminished in mice treated with C1-27. H&E photomicrographs from the midsegment of mouse colons from control, C1-27-treated, and GSTO1-1$^{-/-}$ mice identified this region of the bowel with the most intense active inflammation (Figure S3). GSTO1-1$^{-/-}$ mice exposed to DSS were associated with prominent submucosal edema (Figure S3D, blue bracket). Wild-type (WT) mice exposed to DSS were injected daily with 50 mg/kg C1-27, and they showed more submucosal edema but displayed similar levels of inflammatory cell infiltrate compared with WT mice exposed to DSS alone

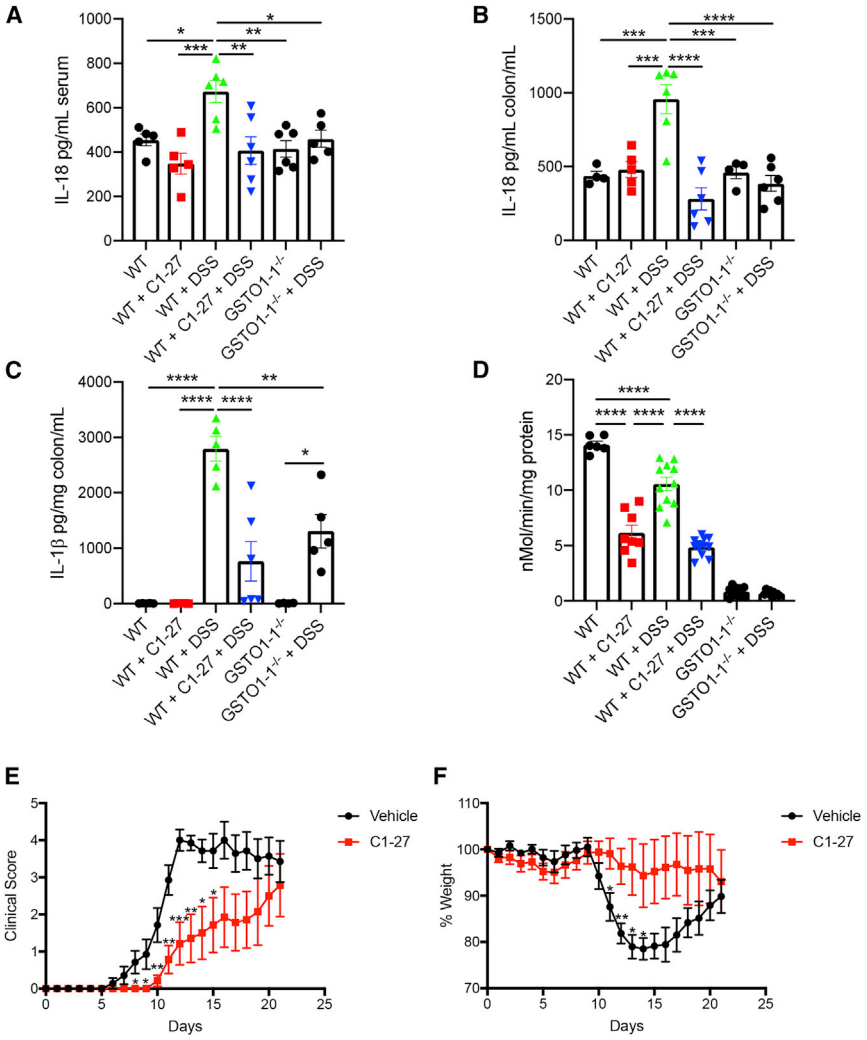

Figure 3. C1-27 Is Active *In Vivo* and Reduces Inflammasome Activation Associated with DSS-Induced Colitis and EAE Development

Mice were treated with azoxymethane (AOM) 7.5 mg/kg intraperitoneally (i.p.) at day −3. On day 0, DSS 2.5% was included in drinking water. C1-27 was introduced by daily i.p. injection at a dose of 50 mg/kg in 40% cyclodextrin from day −1 until day 7. Mice were sacrificed and samples collected on day 8.

(A) Serum IL-18 levels (n = 5–6).

(B) Colon culture supernatant IL-18 levels (n = 5–6).

(C) Colon culture supernatant IL-1β levels (n = 5–6).

(D) Liver GSTO1-1 activity with S-(4-nitrophenacyl) glutathione (4NPG; n = 8–12).

(E) Clinical score after EAE induction of C57BL/6 mice injected daily with 40% cyclodextrin/PBS vehicle control or 50 mg/kg C1-27 (n = 7).

(F) C57BL/6 mice treated in (E) were weighed daily. Percentage weight was calculated from starting weight of mice (n = 7).

Data are mean ± SEM; p values calculated using Student's t test or one-way ANOVA with Sidak's multiple comparisons test (*p < 0.05, **p < 0.01, ***p < 0.001, ****p < 0.0001).

(Figure S3, compare Figure S3C to Figure S3B). The active chronic inflammation caused thickening of the bowel in the DSS-treated mice (Figure S3B). Inflammation was seen in the mucosa and submucosa and variably extended through the muscularis propria (Figures S3B–S3D). This supports the contention that C1-27 mediates its effect on the release of IL-1β and IL-18 by modulating the activity of GSTO1-1.

We next assessed if C1-27 could limit inflammation in the NLRP3-dependent experimental autoimmune encephalomyelitis (EAE) model (Gris et al., 2010; Jha et al., 2010). Mice injected daily with 50 mg/kg C1-27 had significantly delayed onset of EAE and had an overall reduced clinical score (Figure 3E). Further, mice injected with C1-27 maintained body weight compared to vehicle controls (Figure 3F). These data support that C1-27 is active *in vivo* and limits EAE induction.

GSTO1-1$^{-/-}$ Mice Have Impaired NLRP3 Inflammasome Activation

We next assessed whether macrophages from GSTO1-1$^{-/-}$ mice would also have impaired NLRP3 inflammasome activation. No difference was observed in the expression of NLRP3 inflammasome components in either unstimulated or LPS-treated BMDMs compared to control mice (Figure 4A). GSTO1-1 deficiency was confirmed by immunoblotting (Figure 4A, fifth panel) and RNA expression (Figure 4B). Peritoneal exudate cells (PECs) from GSTO1-1$^{-/-}$ mice confirmed impairment of NLRP3 inflammasome activation in response to LPS and nigericin treatment, with reduced release of mature caspase-1 p20 and mature IL-1β p17 secretion into the supernatant (Figure 4C, supernatant panels, compare lane 6 to lane 3). GSTO1-1$^{-/-}$ PECs also had impaired IL-1β secretion confirmed by ELISA (Figure 4D). GSTO1-1$^{-/-}$ BMDMs exhibited reduced NLRP3 inflammasome activation, with less mature caspase-1 p20 and mature IL-1β p17 detected in the supernatant (Figure 4E, supernatant panels, compare lane 8 to lane 4). IL-1β secretion detected by ELISA was also significantly reduced in GSTO1-1$^{-/-}$ BMDMs (Figure 4F). Similar to C1-27, cell death resulting from LPS and ATP stimulation was reduced in GSTO1-1$^{-/-}$ BMDMs (Figure 4G). We established that the inhibitory effect of GSTO1-1 knockout was specific to the NLRP3 inflammasome as AIM2 inflammasome activation was unaffected in GSTO1-1$^{-/-}$ BMDMs, as measured by IL-1β release (Figure S4A) and caspase-1 and IL-1β processing (Figure S4B, supernatant panels, compare lane 8 to lane 4). To confirm that the effect of C1-27 is due to inhibition of GSTO1-1 during inflammasome activation, we added two concentrations of C1-27 to WT and GSTO1-1$^{-/-}$ BMDMs. C1-27 significantly inhibited IL-1β release from WT BMDMs but was unable to further reduce IL-1β release from GSTO1-1$^{-/-}$ BMDMs

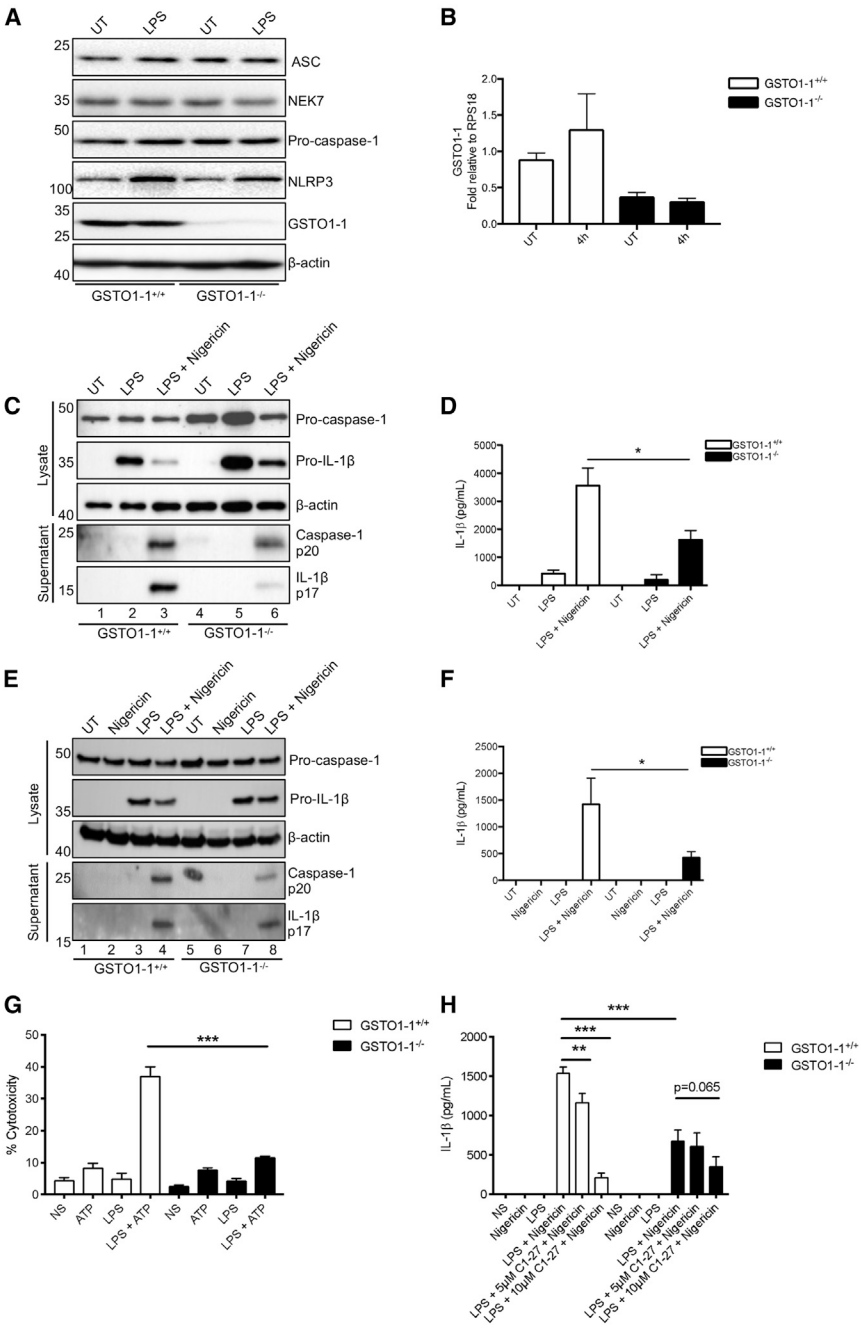

Figure 4. GSTO1-1$^{-/-}$ Mice Have Impaired NLRP3 Inflammasome Activation

(A) Immunoblot of WT and GSTO1-1$^{-/-}$ BMDMs treated with 100 ng/mL LPS for 4 h (n = 3).

(B) qRT-PCR analysis of WT and GSTO1-1$^{-/-}$ BMDMs primed with 100 ng/mL LPS for 4 h. Samples were reverse transcribed and control (Ct) values used for quantification relative to control RPS18 gene (n = 3).

(C) Immunoblot of WT and GSTO1-1$^{-/-}$ PECs primed with 100 ng/mL LPS for 3 h and stimulated with 10 μM nigericin for 45 min (n = 3).

(D) ELISA of IL-1β in the supernatants from PECs treated in (C) (n = 3).

(E) Immunoblot of WT and GSTO1-1$^{-/-}$ BMDMs primed with 100 ng/mL LPS for 3 h and stimulated with 10 μM nigericin for 45 min (n = 3).

(F) ELISA of IL-1β in the supernatants from BMDMs treated in (E) (n = 3).

(G) % Cytotoxicity from WT and GSTO1-1$^{-/-}$ BMDMs primed with 100 ng/mL LPS for 3 h and stimulated with 5 mM ATP for 45 min (n = 3).

(H) ELISA of IL-1β in the supernatants from WT and GSTO1-1$^{-/-}$ BMDMs primed with 100 ng/mL LPS for 3 h, treated with indicated doses of C1-27 for 45 min, and stimulated with 10 μM nigericin for 45 min (n = 3).

Data are mean ± SEM; p values calculated using one-way ANOVA with Sidak's multiple comparisons test (*p < 0.05, **p < 0.01).

(Figure S4E). GSTO1-1 knockdown cells exhibited normal responses to LPS, including induction of mRNA for IL-1β (Figure S4F), NLRP3 (Figure S4G), or the cytokines IL-6 (Figure S4H) and TNF-α (Figure S4I). Overall, the use of the GSTO1-1 inhibitor C1-27, siRNA to GSTO1-1, and GSTO1-1$^{-/-}$ macrophages indicate a regulatory role for GSTO1-1 in NLRP3 inflammasome activation.

NLRP3 Inflammasome Activation Is Augmented in the Presence of GSTO1-1 and Limited by Exogenous GSH

We next assessed the functional role for GSTO1-1 during NLRP3 inflammasome activation using a standard reconstitution system in HEK293T cells (Shi et al., 2016a). Reconstitution of the NLRP3 inflammasome in the presence of GSTO1-1 significantly increased IL-1β secretion detected by ELISA (Figure 5A, compare histobar 3 to histobar 2). Overexpression of GSTO1-1 did not alter expression of pro-caspase-1 (Figure 5B, top panel). A role for GSTO1-1 suggests deglutathionylation as a possible process required for NLRP3 activation. We therefore next assessed if addition of exogenous GSH could limit NLRP3 inflammasome activation in BMDMs. Using a cell-permeable ethyl-ester GSH (GSH-EE) (Anderson et al., 1985), added after LPS priming, IL-1β secretion in response to LPS and ATP

(Figure 4H), indicating that the effect of C1-27 was through inhibition of GSTO1-1. We also tested if endogenous knockdown of GSTO1-1 in BMDMs would recapitulate the effects of C1-27 and GSTO1-1 deficiency on NLRP3 inflammasome inhibition. Using a small interfering RNA (siRNA)-mediated approach, GSTO1-1 was efficiently knocked down in BMDMs (Figures S4C and S4D, second panel, compare lanes 5–8 to 1–4). In response to LPS and ATP stimulation, GSTO1-1 knockdown cells had reduced mature caspase-1 p20 and mature IL-1β p17 secretion into the supernatant (Figure S4D, supernatant panels, compare lane 8 to lane 4). Reduced IL-1β secretion was also confirmed by ELISA

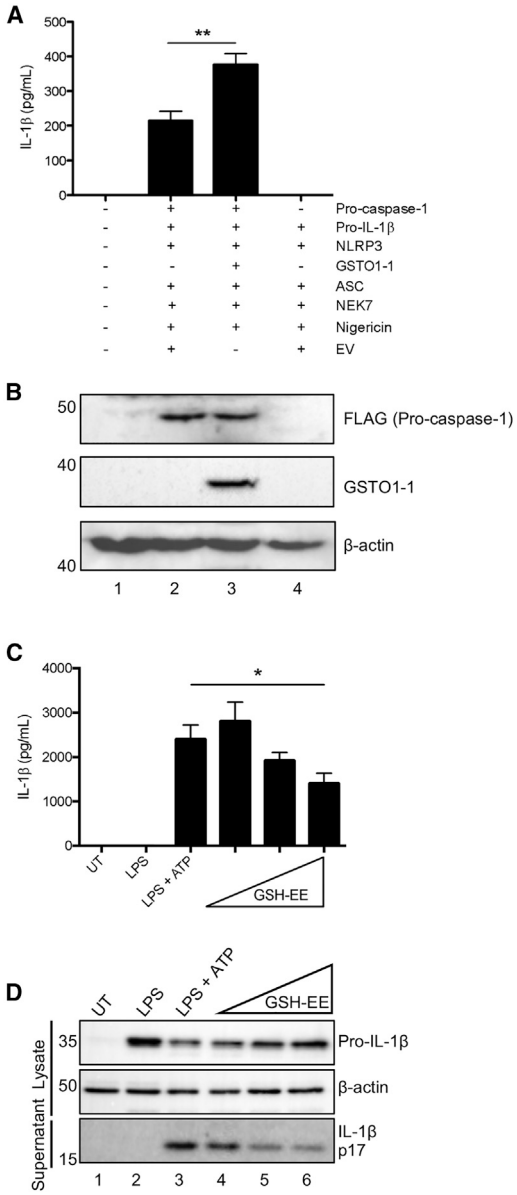

Figure 5. GSTO1-1 Enhances NLRP3 Inflammasome Reconstitution and NLRP3 Activation Is Limited by Exogenous GSH

(A) ELISA of IL-1β secreted by HEK293T cells transiently transfected with plasmids encoding pro-caspase-1, pro-IL-1β, NLRP3, ASC, NEK7, and GSTO1-1 and stimulated with 10 μM nigericin. DNA concentration was kept constant using the relevant empty vector control (n = 3).

(B) Immunoblot of HEK293T cells transfected in (A) (n = 3).

(C) ELISA of IL-1β in the supernatants from BMDMs primed with LPS for 3 h, incubated with GSH-EE (1 mM, 5 mM, or 10 mM) for 45 min, and stimulated with 5 mM ATP for 45 min (n = 3).

(D) Immunoblot of BMDMs treated in (C) (n = 3).

Data are mean ± SEM; p values calculated using one-way ANOVA with Sidak's multiple comparisons test (*p < 0.05, **p < 0.01).

stimulation was significantly reduced (Figure 5C). GSH-EE dose-dependently increased the levels of pro-IL-1β (Figure 5D, lysate panel, compare lanes 4–6 to lane 3) and also reduced secretion of mature IL-1β p17 into the supernatant (Figure 5D, supernatant panel, compare lanes 4–6 to lane 3).

GSTO1-1 Regulates the NLRP3 Inflammasome through Deglutathionylation of NEK7 on Cysteine 253

The question arose as to how GSTO1-1 might be regulating the NLRP3 inflammasome. NEK7 has been recently identified as an NLRP3 inflammasome component, as it senses ROS to promote NEK7-NLRP3 interaction (Shi et al., 2016b). We therefore examined if GSTO1-1 might interact with NEK7. NEK7 co-immunoprecipitated with GSTO1-1 (Figure 6A, upper panel, compare lane 3 to lane 1). An interaction with ASC was also observed (lane 2). We were unable to detect an interaction between GSTO1-1 and NLRP3 by immunoprecipitation (data not shown). GSTO1-1 was unlikely to be regulating ASC, as ASC is utilized by the AIM2 and NLRC4 inflammasomes and C1-27 did not limit their activation. We therefore examined NEK7 as a potential GSTO1-1 target. NEK7 is highly conserved between mouse and human, with no variation in cysteine amino acid conservation (Figure S5, the asterisk denotes cysteine residues). Using a specific antibody that recognizes the glutathionylation-glutathione (SSG) motif, we found that NEK7 is a glutathionylated protein as detected by immunoblotting (Figure 6B, upper panel, lane 2). We next examined if GSTO1-1 and NEK7 could interact endogenously. Using BMDMs, we identified an endogenous interaction between NEK7 and GSTO1-1 during LPS and ATP stimulation (Figure 6C, upper panel, lane 2). Endogenous immunoprecipitation of NEK7 from WT and GSTO1-1$^{-/-}$ BMDMs and subsequent immunoblotting for GSH revealed that NEK7 was deglutathionylated upon LPS and ATP stimulation in WT BMDMs (Figure 6D, upper panel, lane 3). In contrast, NEK7 was still highly glutathionylated upon LPS and ATP stimulation in GSTO1$^{-/-}$ BMDMs (Figure 6D, upper panel, lane 7), suggesting that GSTO1-1 is required for NEK7 deglutathionylation. To formally evaluate the strength of the NEK7-GSTO1-1 interaction, we performed direct binding studies using surface plasmon resonance. WT GSTO1-1 exhibited moderate binding to NEK7 with a disassociation constant (K_D) of 60 ± 4 μM. Notably, mutation of a catalytic cysteine (C32A) that enables GSTO1-1 mediated deglutathionylation resulted in a 2-fold decrease in the binding strength with a K_D of 120.5 ± 0.25 μM (Figures 6E and 6F). This suggests that C32 is involved in the interaction with NEK7, possibly modulating its functional outcome.

To examine NEK7 cysteine glutathionylation, we overexpressed hemagglutinin (HA)-tagged NEK7 in HEK293T cells and used mass spectrometry to identify GSH adducts. Tandem mass spectrometry of immunoprecipitated NEK7 identified NEK7 peptides with GSH adducts on cysteines 79 and 253 (Figures S6A and S6B). We next generated NEK7 cysteine to alanine mutants by site-directed mutagenesis and reconstituted the NLRP3 inflammasome using the mutants to assess pro-IL-1β processing. NEK7 mutants were adequately expressed in each condition (Figure 6G). IL-1β secretion was comparable between each cysteine to alanine mutant, with exception of NEK7 C253A, which significantly enhanced IL-1β processing comparable to WT NEK7 (Figure 6H, compare histobar 2 to histobar 1). These data suggest that deglutathionylation of NEK7 on cysteine 253 might boost NEK7 function in relation to NLRP3 activation.

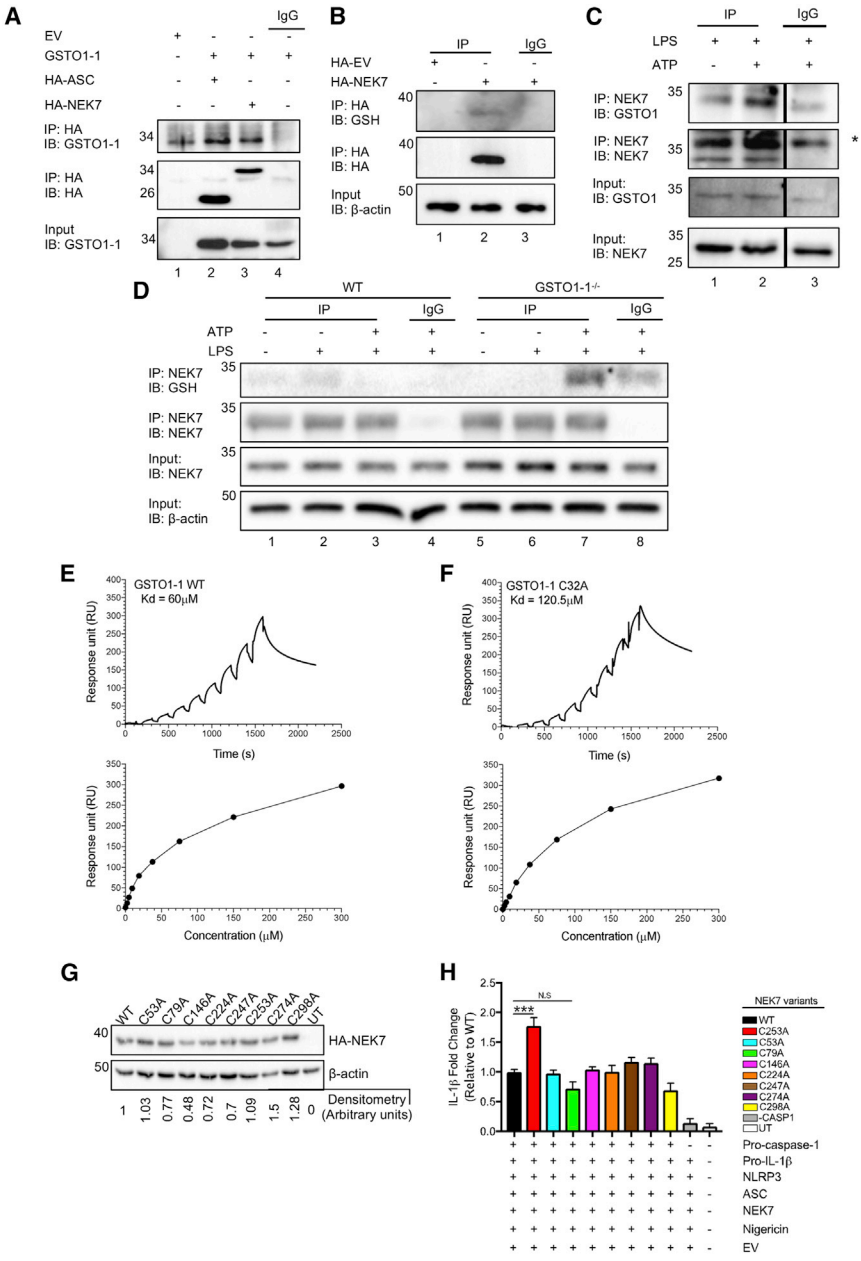

Figure 6. NEK7 Deglutathionylation by GSTO1-1 Promotes NLRP3 Activation

(A) Co-immunoprecipitation of HEK293T cells transiently transfected with Myc-DDK-GSTO1-1, HA-ASC, or HA-NEK7 plasmids. DNA concentration was kept constant using the relevant empty vector control. Immunoprecipitated complexes were analyzed by immunoblot (n = 3).

(B) Non-reducing immunoprecipitation of HEK293T cells transiently transfected with HA-NEK7 plasmid or relevant empty vector control. Immunoprecipitated samples were harvested in lysis buffer containing 50 mM N-ethylmaleimide, and immunoprecipitated complexes were eluted in sample buffer without DTT. Immunoprecipitated samples were analyzed by immunoblot (n = 3).

(C) Endogenous co-immunoprecipitation of NEK7 and GSTO1-1 from primary BMDMs. BMDMs were primed with LPS for 3 h and stimulated with 5 mM ATP for 45 min. Immunoprecipitated complexes were eluted using 5X sample loading buffer (containing DTT) and analyzed by immunoblot. * denotes non-specific band (n = 3).

(D) Endogenous non-reducing immunoprecipitation of NEK7 from WT and GSTO1-1$^{-/-}$ BMDMs primed with 100 ng/ml LPS for 3 h and subsequently treated with 5 mM ATP for 15 min. Immunoprecipitated samples were harvested in lysis buffer containing 50 mM N-ethylmaleimide, and immunoprecipitated complexes were eluted in sample buffer without DTT. Immunoprecipitated samples were analyzed by immunoblot (n = 1).

(E and F) The affinity of NEK7-GSTO1-1 WT (E) and NEK7-GSTO1-1 C32A (F) interaction was determined by surface plasmon resonance by measuring the graded concentration of GSTO1-1 (up to 300 μM). Top panel: binding of GSTO1-1 wild-type and mutant to the immobilized NEK7 presented as a response unit (RU) after subtraction from the reference flow cell. Bottom panel: saturation plot curve for the respective interactions (n = 4).

(G) Immunoblot of HEK293T cells transfected with HA-NEK7 WT or HA-NEK7 cysteine to alanine mutants. Samples were analyzed by immunoblot using anti-HA antibody (n = 3). Densitometry was performed using a representative blot.

(H) ELISA of IL-1β secreted into the supernatant of HEK293T cells transiently transfected with NLRP3 inflammasome components, or NEK7 cysteine to alanine mutants and stimulated with 10 μM nigericin. DNA concentration was kept constant by addition of relevant empty vector control (n = 3).

Data are mean ± SEM; p values calculated using one-way ANOVA with Sidak's multiple comparisons test (***p < 0.001).

Overall, our data point to a key role for the deglutathionylating enzyme GSTO1-1 in the regulation of the NLRP3 inflammasome, with NEK7 being a key target for deglutathionylation.

DISCUSSION

In this study, we provide evidence for GSTO1-1 as a regulator of the NLRP3 inflammasome. It has previously been reported that GSTO1-1$^{-/-}$ mice produced less serum IL-1β in response to *in vivo* LPS treatment (Menon et al., 2017), possibly pointing to GSTO1-1 as an important NLRP3 regulator. In 2003, Laliberte et al. (2003) identified sulfonylurea-containing compounds termed CRIDs as potential inhibitors of IL-1β secretion. CRIDs were found to limit processing of IL-1β in human monocytes, and mice given oral CRIDs had attenuated production of IL-1β in response to LPS and ATP, with no effect on IL-6 or TNF-α. Further analysis identified GSTO1-1 as a potential CRID target by affinity labeling of GSTO1-1 with radioactive CRID1 and CRID2. We initially hypothesized that GSTO1-1 might be the target for MCC950, a derivative of

CRID2 (Coll et al., 2015), which we previously reported to be a highly potent and selective NLRP3 inhibitor. We found that MCC950 was a poor GSTO1-1 inhibitor, with an IC_{50} of 124.8 μM, compared to the more potent C1-27, which had been found in an unbiased screen of GSTO1-1 inhibitors (Ramkumar et al., 2016) and had an IC_{50} of 44.5nM. We therefore concluded that MCC950 was unlikely to be targeting GSTO1-1 to regulate the NLRP3 inflammasome. However, our evidence here implicates GSTO1-1 as an NLRP3 inflammasome regulator, limiting both canonical and non-canonical inflammasome-mediated pro-IL-1β processing. Pre-treatment with C1-27 also reduced pro-IL-1β expression in LPS-stimulated BMDMs, which may be due to an additional inhibitory effect occurring independently of nuclear factor κB (NF-κB) activation. This effect was not replicated in GSTO1-$1^{-/-}$ BMDMs. A previous study concerning MCC950 suggested a lack of a role for GSTO1-1 in NLRP3 activation, as GSTO1-1 knockdown in immortalized macrophages had no effect on NLRP3 activation (Primiano et al., 2016). Our study, however, using both GSTO1-1 knockdown and knockout approaches implicate GSTO1-1 as an NLRP3 regulator. The basis for this discrepancy is not clear but may perhaps be due to the use of immortalized cells compared to primary cells.

The question arose as to how GSTO1-1 might be regulating the NLRP3 inflammasome. GSTO1-1 has a proinflammatory function *in vivo*, as both C1-27-treated mice and GSTO1-$1^{-/-}$ mice showed decreased IL-18 and IL-1β secretion in a DSS-induced colitis model of inflammation, although histological staining actually identified increased neutrophil infiltration and inflammation. Further, C1-27 reduced ASC speck formation, suggesting that GSTO1-1 functions upstream of caspase-1 activation during inflammasome assembly. Due to the observed lack of inhibition by C1-27 during AIM2 and NLRC4 inflammasome activation, we hypothesized that GSTO1-1 was regulating NLRP3 or NEK7 in a GSH-dependent mechanism. GSTO1-1-deficient macrophages have increased cellular glutathionylation, indicating GSTO1-1 serves as a deglutathionylating enzyme (Menon and Board, 2013). It should, however, be mentioned that cells possess multiple glutathionylation and deglutathionylation systems, such as the glutaredoxin system, and the potential that these systems are also contributing to inflammasome modulation cannot be ruled out. Despite a previous finding identifying NLRP3 as a glutathionylated protein (Guglielmo et al., 2017), we were unable to detect glutathionylation of NLRP3 by immunoprecipitation or mass spectrometry (data not shown). NEK7 was recently identified as a ROS-sensing component of the NLRP3 inflammasome, as treatment of cells with N-acetylcysteine, a GSH precursor, inhibited NEK7-NLRP3 interaction (Shi et al., 2016b). Similarly, we found that pre-treatment with a cell-permeable ethyl-ester form of GSH limited NLRP3 inflammasome activation. The kinase activity of NEK7 was dispensable for NLRP3 inflammasome activation, indicating that NEK7 may act as a scaffold for inflammasome activation (Shi et al., 2016b). Supporting this finding, oridonin, an inhibitor of the NLRP3 NACHT domain on cysteine 279, was shown to block NLRP3-NEK7 interaction, preventing NLRP3 inflammasome assembly (He et al., 2018). Furthermore, cryo-electron microscopy revealed NEK7-NLRP3 interaction at 3.8 Å (Sharif et al., 2019). We found that NEK7 was glutathionylated on cysteines 79 and 253 and that GSTO1-1 and NEK7 interacted by overexpression, endogenously, and by surface plasmon resonance. As NEK7 and GSTO1-1 interacted more upon inflammasome activation, NEK7 was deglutathionylated—this did not occur in GSTO1-$1^{-/-}$ BMDMs, where NEK7 remained highly glutathionylated upon inflammasome activation, suggesting that the deglutathionylation was indeed GSTO1-1 dependent. A previous report showed that caspase-1 is glutathionylated, thereby limiting inflammasome activation (Meissner et al., 2008). Our data indicate that NEK7 is also glutathionylated, which similarly limits NLRP3 inflammasome activation. Mutagenesis of C253 in NEK7 to alanine increased IL-1β processing, indicating negative regulation of NEK7 by C253 modification. Importantly, activation of the NLRP3 inflammasome was significantly enhanced in the presence of GSTO1-1 by reconstitution, implicating GSTO1-1 as a regulator of NLRP3 inflammasome activation.

Taken together, our data therefore identify GSTO1-1 as a NLRP3 inflammasome regulator acting via deglutathionylation of C253 in NEK7. Interestingly, neurological disorders, such as Alzheimer's disease, exhibit underlying oxidative imbalance. The levels of GSH decrease as we age (Liu and Choi, 2000; Saharan and Mandal, 2014), and pathological NLRP3 activation has recently been identified as a driver of Alzheimer's disease (Heneka et al., 2013; Yin et al., 2018). Polymorphisms in the gene encoding GSTO1-1 have been previously linked to progression of Alzheimer's disease (Li et al., 2003; Umlauf et al., 2016). Targeting GSTO1-1 with agents such as C1-27 may have therapeutic benefits in limiting aberrant NLRP3 activation in neurological diseases such as Alzheimer's disease and multiple sclerosis (MS), indicated here from the inhibitory effect of C1-27 on EAE. Development of novel GSTO1-1 inhibitors may hold promise in the treatment of NLRP3-mediated inflammatory diseases.

STAR★METHODS

Detailed methods are provided in the online version of this paper and include the following:

- KEY RESOURCES TABLE
- LEAD CONTACT AND MATERIALS AVAILABILITY
- EXPERIMENTAL MODEL AND SUBJECT DETAILS
  - In vivo animal models
  - In vitro models
- METHOD DETAILS
  - Inflammasome assays
  - LPS Transfection
  - LDH release assay
  - Immunoprecipitations
  - RNA extraction and qPCR
  - Disuccinimidyl suberate crosslinking
  - Confocal Microscopy
  - Colon organ culture
  - Histological Analysis

SUPPLEMENTAL INFORMATION

Supplemental Information can be found online at https://doi.org/10.1016/j.celrep.2019.08.072.

ACKNOWLEDGMENTS

We would like to thank Dr. Rebecca Coll and Dr. Deepthi Menon for helpful discussions. We would like to thank FingerPrints Proteomics Facility in the University of Dundee for mass spectrometry analysis and Ms. Elaine Bean from ACT Pathology, Canberra Hospital who processed the samples for histological analysis. We would like to acknowledge the following grants: the National Health and Medical Research Council of Australia (NHMRC) is thanked for Project Grant APP1124673 to P.G.B., M.G.C., and L.A.J.O.; Principal Research Fellowship 1117602 to J.B.B.; and NHMRC Project Grant APP1156455 to J.B.B., P.G.B., and M.G.C. The O'Neill laboratory acknowledges the following grant support: European Research Council (ECFP7-ERC-MICROINNATE) and Science Foundation Ireland Investigator Award (SFI 12/IA/1531).

AUTHOR CONTRIBUTIONS

M.M.H. and L.A.J.O. designed the study. M.M.H., A.H., S.A., P.T., M.C.R., Z.Z., C.E.S., E.M.P.-M., C.D., M.C.R., S.T., S.S., M.G.C., J.E.D., P.G.B., A.F.M., and S.C.C. performed experiments. M.M.H., A.H., S.A., E.M.P.-M., C.D., C.E.S., P.T., J.E.D., and P.G.B. analyzed data. N.N., Y.X., and J.B.B. synthesized and supplied C1-27. R.J.S.P., P.G.B., and K.H.G.M. provided critical input. M.M.H., A.H., and L.A.J.O. wrote the manuscript with input from the authors.

DECLARATION OF INTERESTS

The authors declare no competing interests.

Received: September 20, 2018
Revised: July 31, 2019
Accepted: August 23, 2019
Published: October 1, 2019

REFERENCES

Allen, I.C., TeKippe, E.M., Woodford, R.M., Uronis, J.M., Holl, E.K., Rogers, A.B., Herfarth, H.H., Jobin, C., and Ting, J.P. (2010). The NLRP3 inflammasome functions as a negative regulator of tumorigenesis during colitis-associated cancer. J. Exp. Med. *207*, 1045–1056.

Anderson, M.E., Powrie, F., Puri, R.N., and Meister, A. (1985). Glutathione monoethyl ester: preparation, uptake by tissues, and conversion to glutathione. Arch. Biochem. Biophys. *239*, 538–548.

Baker, R.T., Catanzariti, A.M., Karunasekara, Y., Soboleva, T.A., Sharwood, R., Whitney, S., and Board, P.G. (2005). Using deubiquitylating enzymes as research tools. Methods Enzymol. *398*, 540–554.

Board, P.G., Coggan, M., Cappello, J., Zhou, H., Oakley, A.J., and Anders, M.W. (2008). S-(4-Nitrophenacyl)glutathione is a specific substrate for glutathione transferase omega 1-1. Anal. Biochem. *374*, 25–30.

Coll, R.C., Robertson, A., Butler, M., Cooper, M., and O'Neill, L.A. (2011). The cytokine release inhibitory drug CRID3 targets ASC oligomerisation in the NLRP3 and AIM2 inflammasomes. PLoS ONE *6*, e29539.

Coll, R.C., Robertson, A.A., Chae, J.J., Higgins, S.C., Muñoz-Planillo, R., Inserra, M.C., Vetter, I., Dungan, L.S., Monks, B.G., Stutz, A., et al. (2015). A small-molecule inhibitor of the NLRP3 inflammasome for the treatment of inflammatory diseases. Nat. Med. *21*, 248–255.

Domingo-Fernández, R., Coll, R.C., Kearney, J., Breit, S., and O'Neill, L.A.J. (2017). The intracellular chloride channel proteins CLIC1 and CLIC4 induce IL-1β transcription and activate the NLRP3 inflammasome. J. Biol. Chem. *292*, 12077–12087.

Fink, S.L., and Cookson, B.T. (2006). Caspase-1-dependent pore formation during pyroptosis leads to osmotic lysis of infected host macrophages. Cell. Microbiol. *8*, 1812–1825.

Gris, D., Ye, Z., Iocca, H.A., Wen, H., Craven, R.R., Gris, P., Huang, M., Schneider, M., Miller, S.D., and Ting, J.P. (2010). NLRP3 plays a critical role in the development of experimental autoimmune encephalomyelitis by mediating Th1 and Th17 responses. J. Immunol. *185*, 974–981.

Groß, C.J., Mishra, R., Schneider, K.S., Médard, G., Wettmarshausen, J., Dittlein, D.C., Shi, H., Gorka, O., Koenig, P.A., Fromm, S., et al. (2016). K^+ Efflux-Independent NLRP3 Inflammasome Activation by Small Molecules Targeting Mitochondria. Immunity *45*, 761–773.

Guglielmo, A., Sabra, A., Elbery, M., Cerveira, M.M., Ghenov, F., Sunasee, R., and Ckless, K. (2017). A mechanistic insight into curcumin modulation of the IL-1β secretion and NLRP3 S-glutathionylation induced by needle-like cationic cellulose nanocrystals in myeloid cells. Chem. Biol. Interact. *274*, 1–12.

He, Y., Zeng, M.Y., Yang, D., Motro, B., and Núñez, G. (2016). NEK7 is an essential mediator of NLRP3 activation downstream of potassium efflux. Nature *530*, 354–357.

He, H., Jiang, H., Chen, Y., Ye, J., Wang, A., Wang, C., Liu, Q., Liang, G., Deng, X., Jiang, W., and Zhou, R. (2018). Oridonin is a covalent NLRP3 inhibitor with strong anti-inflammasome activity. Nat. Commun. *9*, 2550.

Heneka, M.T., Kummer, M.P., Stutz, A., Delekate, A., Schwartz, S., Vieira-Saecker, A., Griep, A., Axt, D., Remus, A., Tzeng, T.C., et al. (2013). NLRP3 is activated in Alzheimer's disease and contributes to pathology in APP/PS1 mice. Nature *493*, 674–678.

Hornung, V., Ablasser, A., Charrel-Dennis, M., Bauernfeind, F., Horvath, G., Caffrey, D.R., Latz, E., and Fitzgerald, K.A. (2009). AIM2 recognizes cytosolic dsDNA and forms a caspase-1-activating inflammasome with ASC. Nature *458*, 514–518.

Hughes, M.M., Lavrencic, P., Coll, R.C., Ve, T., Ryan, D.G., Williams, N.C., Menon, D., Mansell, A., Board, P.G., Mobli, M., et al. (2017). Solution structure of the TLR adaptor MAL/TIRAP reveals an intact BB loop and supports MAL Cys91 glutathionylation for signaling. Proc. Natl. Acad. Sci. USA *114*, E6480–E6489.

Jha, S., Srivastava, S.Y., Brickey, W.J., Iocca, H., Toews, A., Morrison, J.P., Chen, V.S., Gris, D., Matsushima, G.K., and Ting, J.P. (2010). The inflammasome sensor, NLRP3, regulates CNS inflammation and demyelination via caspase-1 and interleukin-18. J. Neurosci. *30*, 15811–15820.

Juliana, C., Fernandes-Alnemri, T., Kang, S., Farias, A., Qin, F., and Alnemri, E.S. (2012). Non-transcriptional priming and deubiquitination regulate NLRP3 inflammasome activation. J. Biol. Chem. *287*, 36617–36622.

Kayagaki, N., Warming, S., Lamkanfi, M., Vande Walle, L., Louie, S., Dong, J., Newton, K., Qu, Y., Liu, J., Heldens, S., et al. (2011). Non-canonical inflammasome activation targets caspase-11. Nature *479*, 117–121.

Laliberte, R.E., Perregaux, D.G., Hoth, L.R., Rosner, P.J., Jordan, C.K., Peese, K.M., Eggler, J.F., Dombroski, M.A., Geoghegan, K.F., and Gabel, C.A. (2003). Glutathione s-transferase omega 1-1 is a target of cytokine release inhibitory drugs and may be responsible for their effect on interleukin-1beta posttranslational processing. J. Biol. Chem. *278*, 16567–16578.

Li, Y.J., Oliveira, S.A., Xu, P., Martin, E.R., Stenger, J.E., Scherzer, C.R., Hauser, M.A., Scott, W.K., Small, G.W., Nance, M.A., et al. (2003). Glutathione

S-transferase omega-1 modifies age-at-onset of Alzheimer disease and Parkinson disease. Hum. Mol. Genet. *12*, 3259–3267.

Liu, R., and Choi, J. (2000). Age-associated decline in gamma-glutamylcysteine synthetase gene expression in rats. Free Radic. Biol. Med. *28*, 566–574.

Lu, A., Magupalli, V.G., Ruan, J., Yin, Q., Atianand, M.K., Vos, M.R., Schröder, G.F., Fitzgerald, K.A., Wu, H., and Egelman, E.H. (2014). Unified polymerization mechanism for the assembly of ASC-dependent inflammasomes. Cell *156*, 1193–1206.

Martinon, F., Burns, K., and Tschopp, J. (2002). The inflammasome: a molecular platform triggering activation of inflammatory caspases and processing of proIL-beta. Mol. Cell *10*, 417–426.

Masumoto, J., Taniguchi, S., Ayukawa, K., Sarvotham, H., Kishino, T., Niikawa, N., Hidaka, E., Katsuyama, T., Higuchi, T., and Sagara, J. (1999). ASC, a novel 22-kDa protein, aggregates during apoptosis of human promyelocytic leukemia HL-60 cells. J. Biol. Chem. *274*, 33835–33838.

Meissner, F., Molawi, K., and Zychlinsky, A. (2008). Superoxide dismutase 1 regulates caspase-1 and endotoxic shock. Nat. Immunol. *9*, 866–872.

Menon, D., and Board, P.G. (2013). A role for glutathione transferase Omega 1 (GSTO1-1) in the glutathionylation cycle. J. Biol. Chem. *288*, 25769–25779.

Menon, D., Coll, R., O'Neill, L.A., and Board, P.G. (2014). Glutathione transferase omega 1 is required for the lipopolysaccharide-stimulated induction of NADPH oxidase 1 and the production of reactive oxygen species in macrophages. Free Radic. Biol. Med. *73*, 318–327.

Menon, D., Innes, A., Oakley, A.J., Dahlstrom, J.E., Jensen, L.M., Brüstle, A., Tummala, P., Rooke, M., Casarotto, M.G., Baell, J.B., et al. (2017). GSTO1-1 plays a pro-inflammatory role in models of inflammation, colitis and obesity. Sci. Rep. *7*, 17832.

Mladenova, D., Daniel, J.J., Dahlstrom, J.E., Bean, E., Gupta, R., Pickford, R., Currey, N., Musgrove, E.A., and Kohonen-Corish, M.R. (2011). The NSAID sulindac is chemopreventive in the mouse distal colon but carcinogenic in the proximal colon. Gut *60*, 350–360.

Primiano, M.J., Lefker, B.A., Bowman, M.R., Bree, A.G., Hubeau, C., Bonin, P.D., Mangan, M., Dower, K., Monks, B.G., Cushing, L., et al. (2016). Efficacy and Pharmacology of the NLRP3 Inflammasome Inhibitor CP-456,773 (CRID3) in Murine Models of Dermal and Pulmonary Inflammation. J. Immunol. *197*, 2421–2433.

Ramkumar, K., Samanta, S., Kyani, A., Yang, S., Tamura, S., Ziemke, E., Stuckey, J.A., Li, S., Chinnaswamy, K., Otake, H., et al. (2016). Mechanistic evaluation and transcriptional signature of a glutathione S-transferase omega 1 inhibitor. Nat. Commun. *7*, 13084.

Saharan, S., and Mandal, P.K. (2014). The emerging role of glutathione in Alzheimer's disease. J. Alzheimers Dis. *40*, 519–529.

Sahillioglu, A.C., Sumbul, F., Ozoren, N., and Haliloglu, T. (2014). Structural and dynamics aspects of ASC speck assembly. Structure *22*, 1722–1734.

Sharif, H., Wang, L., Wang, W.L., Magupalli, V.G., Andreeva, L., Qiao, Q., Hauenstein, A.V., Wu, Z., Núñez, G., Mao, Y., and Wu, H. (2019). Structural mechanism for NEK7-licensed activation of NLRP3 inflammasome. Nature *570*, 338–343.

Shi, H., Murray, A., and Beutler, B. (2016a). Reconstruction of the Mouse Inflammasome System in HEK293T Cells. Bio. Protoc. *6*, e1986.

Shi, H., Wang, Y., Li, X., Zhan, X., Tang, M., Fina, M., Su, L., Pratt, D., Bu, C.H., Hildebrand, S., et al. (2016b). NLRP3 activation and mitosis are mutually exclusive events coordinated by NEK7, a new inflammasome component. Nat. Immunol. *17*, 250–258.

Stutz, A., Kolbe, C.C., Stahl, R., Horvath, G.L., Franklin, B.S., van Ray, O., Brinkschulte, R., Geyer, M., Meissner, F., and Latz, E. (2017). NLRP3 inflammasome assembly is regulated by phosphorylation of the pyrin domain. J. Exp. Med. *214*, 1725–1736.

Tang, T., Lang, X., Xu, C., Wang, X., Gong, T., Yang, Y., Cui, J., Bai, L., Wang, J., Jiang, W., and Zhou, R. (2017). CLICs-dependent chloride efflux is an essential and proximal upstream event for NLRP3 inflammasome activation. Nat. Commun. *8*, 202.

Ullevig, S.L., Kim, H.S., Short, J.D., Tavakoli, S., Weintraub, S.T., Downs, K., and Asmis, R. (2016). Protein S-Glutathionylation Mediates Macrophage Responses to Metabolic Cues from the Extracellular Environment. Antioxid. Redox Signal. *25*, 836–851.

Umlauf, E., Rappold, E., Schiller, B., Fuchs, P., Rainer, M., Wolf, B., and Zellner, M. (2016). Careful neuropsychological testing reveals a novel genetic marker, GSTO1*C, linked to the pre-stage of Alzheimer's disease. Oncotarget *7*, 39108–39117.

Yin, J., Zhao, F., Chojnacki, J.E., Fulp, J., Klein, W.L., Zhang, S., and Zhu, X. (2018). NLRP3 Inflammasome Inhibitor Ameliorates Amyloid Pathology in a Mouse Model of Alzheimer's Disease. Mol. Neurobiol. *55*, 1977–1987.

Yissachar, N., Salem, H., Tennenbaum, T., and Motro, B. (2006). Nek7 kinase is enriched at the centrosome, and is required for proper spindle assembly and mitotic progression. FEBS Lett. *580*, 6489–6495.

Zaki, M.H., Boyd, K.L., Vogel, P., Kastan, M.B., Lamkanfi, M., and Kanneganti, T.D. (2010). The NLRP3 inflammasome protects against loss of epithelial integrity and mortality during experimental colitis. Immunity *32*, 379–391.

Zhang, X., Liu, P., Zhang, C., Chiewchengchol, D., Zhao, F., Yu, H., Li, J., Kambara, H., Luo, K.Y., Venkataraman, A., et al. (2017). Positive Regulation of Interleukin-1β Bioactivity by Physiological ROS-Mediated Cysteine S-Glutathionylation. Cell Rep. *20*, 224–235.

Zhou, R., Yazdi, A.S., Menu, P., and Tschopp, J. (2011). A role for mitochondria in NLRP3 inflammasome activation. Nature *469*, 221–225.

STAR★METHODS

KEY RESOURCES TABLE

REAGENT or RESOURCE	SOURCE	IDENTIFIER
Antibodies		
Anti-IL-1β	R&D	Cat# AF401-NA
Anti-caspase-1	Adipogen	Cat# AG-20B-0042-C100
Anti-NLRP3	Cell Signaling	Cat# D4D8T
Anti-β-actin	Sigma	Cat# 4267
Anti-ASC	Santa Cruz	Cat# Sc-22514-r
Anti-NEK7	Abcam	Cat# Ab133514
Anti-GSTO1-1	Genetex	Cat# GTX118439
Anti-GSH	Virogen	Cat# 101-A-100
Anti-HA	Sigma	Cat# H3663
Anti-FLAG	Sigma	Cat# F1804
Anti-phospho-p38	Cell Signaling	Cat# 9211
Anti-IκBα	Cell Signaling	Cat# 44D4
Anti-phospho-p65	Cell Signaling	Cat# 93H1
Bacterial and Virus Strains		
E.coli BL21(DE3)	Novagen	Cat# 69450
S. typhimurium UK-1 strain	Dr. Sinéad Corr, TCD	N/A
Chemicals, Peptides, and Recombinant Proteins		
ATP	Invivogen	Cat# tlrl-atpl
Nigericin	Invivogen	Cat# tlrl-nig
Poly (dA:dT)	Invivogen	Cat# tlrl-patn
C1-27	Prof. Nouri Neamati, University of Michigan	N/A
Gentamicin	Sigma	Cat# G1397
GSH-EE	Santa Cruz	Cat# 118421-50-4
ProLong Gold antifade reagent with DAPI	Biosciences	Cat# P36931
Ultrapure rough LPS from *E. coli*, serotype EH100	Alexis	Cat# ALX-581-010-L001
HA peptide	Sigma	Cat# 116669750001
FuGENE HD Transfection Reagent	Promega	Cat# E2311
Strataclean Resin	Agilent Technologies	Cat# 400714
Dextran sulfate sodium salt (DSS) Colitis Grade	MP Biomedicals	Cat# 0216011010
S-(4-nitrophenacyl)glutathione	Prof. Philip Board, ANU	N/A
Disuccinimidyl suberate	ThermoFisher	Cat# 21655
Lipofectamine 2000	ThermoFisher	Cat# 11668030
Lipofectamine RNAiMAX	ThermoFisher	Cat# 13778030
Critical Commercial Assays		
Mouse IL-1β DuoSet ELISA	R&D Systems	Cat# DY401
Mouse TNFα DuoSet ELISA	R&D Systems	Cat# DY410
Human IL-1β DuoSet ELISA	R&D Systems	Cat# DY201
Mouse IL-1β Quantikine ELISA	R&D Systems	Cat# MLB00C
Mouse IL-1β ELISA kit	Abcam	Cat# ab216165
Cytotox 96 non-radioactive cytotoxicity assay	Promega	Cat# G1780
Quikchange II site directed mutagenesis kit	Agilent Technologies	Cat# 200521

(*Continued on next page*)

Continued

REAGENT or RESOURCE	SOURCE	IDENTIFIER
Experimental Models: Cell Lines		
HEK293T cells	Sigma	Cat# 12022001
J774.A1 cells	Sigma	Cat# 91051511
Experimental Models: Organisms/Strains		
Mouse: C57BL/6J	Harlan	N/A
Mouse: GSTO1-1$^{-/-}$ 129/SvEv-C57BL/6J	Taconic	Cat# TF1210
Oligonucleotides		
Scramble siRNA	ThermoFisher	Cat# 43908430
GSTO1-1 siRNA	ThermoFisher	Cat# 4390771/s67153
Primer sequences, see Table S1	This paper	N/A
Site directed mutagenesis sequences, see Table S2	This paper	N/A
Recombinant DNA		
Myc-DDK-GSTO1-1	Origene	Cat# pCMV6; MR202949
FLAG-NLRP3	Shi et al., 2016b	Addgene; Cat# 75127
FLAG-Pro-Caspase-1	Shi et al., 2016b	Addgene; Cat# 75128
HA-ASC	Hornung et al., 2009	Addgene; Cat# 41553
FLAG-pro-IL-1β	Shi et al., 2016b	Addgene; Cat# 75131
HA-NEK7	Shi et al., 2016b	Addgene; Cat# 75142
Software and Algorithms		
Graphpad Prism 8.0	Graphpad	https://www.graphpad.com/scientific-software/prism/
Biacore 8000 BIAevaluation software	GE Healthcare	N/A
Mascot search engine	Matrix Science	http://www.matrixscience.com

LEAD CONTACT AND MATERIALS AVAILABILITY

Further information and requests for resources and reagents should be directed to and will be fulfilled by the Lead Contact, Professor Luke O'Neill (laoneill@tcd.ie). Mutant plasmids were generated by site-directed mutagenesis, the sequences for which are available in Table S2. All unique/stable reagents generated in this study are available from the Lead Contact without restriction.

EXPERIMENTAL MODEL AND SUBJECT DETAILS

In vivo animal models

Animal details

All animal procedures were ethically approved by the Trinity College Dublin Animal Research Ethics Committee prior to experimentation, and conformed with the Directive 2010/63/EU of the European Parliament.

Eight- to twelve-week old C57BL/6J (Harlan) and GSTO1-1$^{-/-}$ mice on the C57BL/6J background were bred under specific pathogen-free conditions at Trinity Biomedical Science Institute animal facility. For the DSS study, GSTO1-1$^{-/-}$ 129/SvEv-C57BL/6J mice were obtained from Taconic and were originally derived from 129S-5 ES cells and backcrossed to an albino C57BL/6J strain. GSTO1-1$^{-/-}$ and wild-type mice that had been backcrossed to C57BL/6J mice from Charles River were much less sensitive to DSS and were not used in this study.

DSS-induced colitis model

Mice were treated with Azoxymethane (AOM) 7.5mg/kg ip.at day −3. On day 0, DSS 2.5% was included in drinking water. C1-27 was introduced by daily ip injection at a dose of 50mg/kg in 40% cyclodextrin from day −1 until day 7. Mice were sacrificed and samples collected on day 8.

Experimental autoimmune encephalomyelitis

To induce EAE, 6–8 week old female C57BL/6 mice received subcutaneous immunization with $MOG_{35–55}$ peptide (150μg/mouse) emulsified in complete Freund's adjuvant containing 4mg/mL heat-killed MTB. Mice were injected intraperitoneally with 200ng/mouse pertussis toxin on day 0 and day 2. Mice were injected daily with 50mg/kg C1-27 (40% cyclodextrin/PBS) intraperitoneally. Mice were weighed daily during the trial. EAE disease scores were recorded as follows: grade 0, normal; grade 1, limp tail; grade 2, wobbly gait; grade 3, hind limb weakness; grade 4, hind limb paralysis; and grade 5, tetraparalysis/death.

In vitro models

Culturing primary bone marrow-derived macrophages (BMDMs)

Bone marrow was obtained by flushing the femur, tibia and hip bone of adult mice with a 25-gauge needle. The bone marrow was subsequently resuspended in red cell lysis buffer (Sigma) for 3 minutes before being centrifuged, resuspended, and passed through a 100 μm cell strainer. Cells were cultured in non-tissue culture treated 10cm dishes for 6 days in DMEM supplemented with FCS (10%), penicillin-streptomycin (1%) and L929 supernatant (10%). On day 6, cells were plated at $5x10^5$ cells/mL unless otherwise stated. Peritoneal exudate cells were isolated by peritoneal cavity lavage with sterile PBS.

Culturing HEK293T cells

Cells were cultured in DMEM supplemented with FCS (10%) and penicillin-streptomycin.

Culturing J774.A1 cells

Cells were cultured in DMEM supplemented with FCS (10%) and penicillin-streptomycin.

METHOD DETAILS

Inflammasome assays

BMDMs were seeded at $5x10^5$ cells/mL on 12-well plates and left overnight at 37°C in 5% CO_2 incubator. Cells were treated with LPS (100ng/mL) for 3h. After 3h, media was removed, cells washed with PBS and replaced with serum-free DMEM. The GSTO1-1 inhibitor C1-27 was added for 45min at a concentration of 5 μM unless otherwise stated. Cells were treated with ATP (5mM) or 10 μM Nigericin (10 μM) for 45min for NLRP3 inflammasome activation. Poly (dA:dT) (1 μg) was transfected into cells for 2h using Lipofectamine 2000 for activation of the AIM2 inflammasome. To assess NLRC4 inflammasome activation, *Salmonella typhimurium* UK1 was grown in LB broth at 37°C shaking overnight, and subsequently sub-cultured until OD1. Bacterial innocula were prepared by centrifugation and washed with PBS, followed by reconstitution in DMEM to M.O.I. 20 for an infection assay. On the day of the assay, BMDMs were treated with LPS (100ng/mL) for 3h. Medium was removed and replaced with serum free DMEM containing C1-27 for 45min followed by infection with *S. typhimurium* at M.O.I 20 for 15min. After 15min, gentamicin (50 μg/mL) was added to kill extracellular bacteria for a further 90min. For all assays 500 μL of supernatant was collected and stored for ELISA. The remaining supernatant was incubated with 5 μL of StrataClean Resin beads, briefly vortexed for 1min and centrifuged at 400 x g for 2 min at 4°C. The supernatant was removed, and beads were resuspended in 30 μL 5X sample loading buffer. Cells were lysed in 50 μL 5X sample loading buffer and analyzed by SDS-PAGE.

LPS Transfection

BMDMs were seeded at $5x10^5$ cells/mL on 12-well plates and left overnight at 37°C in 5% CO_2 incubator. Cells were treated with LPS (100ng/mL) for 4h to induce caspase-11 expression. After 4h, medium was removed, and cells were washed with PBS. 1mL of complete medium was added to cells. 2 μL of LPS (1mg/mL) was added to 45.5 μL Opti-MEM medium and vortexed immediately. 2.5 μL RT FuGENE HD transfection reagent was added to the LPS/Opti-MEM, mixed gently and left for 10min RT. 50 μL was added per well and left for 16h before harvesting supernatant for ELISA and LDH assays.

LDH release assay

Supernatants harvested were assessed for LDH release following inflammasome activation. Lactate release was quantified using the Cytotox 96 non-radioactive cytotoxicity assay (Promega) according to manufacturer's instructions.

Immunoprecipitations

BMDMs were seeded at $1x10^6$ cells/ml in 10cm dishes 12h-24h prior to treatment. HEK293T cells were seeded at $2.5x10^5$ cells/mL in 10cm dishes for 24h-36h prior to transfection. In all cases, the amount of plasmid DNA was kept constant in each transfection by using the appropriate amount of empty vector control. 24h post transfection cells were washed with 5mL ice-cold PBS before being transferred directly to ice. Cells were harvested by lysis in 700 μL of low stringency lysis buffer (50mM HEPES pH 7.5, 100mM NaCl, 1mM EDTA, 10% glycerol, 0.5% Nonident P40 (NP-40), 1mM phenylmethylsulfonyl fluoride (PMSF), 11.5 μg/mL aprotinin, 1 μg/mL leupeptin and 1mM sodium orthovanadate) for 15min on ice. For non-reducing immunoprecipitations, N-ethylmaleimide (50mM) was added. Plates were scraped with a cell scraper and lysate transferred into microcentrifuge tubes. Tubes were centrifuged at 21380 x g for 10min at 4°C. Microcentrifuge tubes were prepared with 30 μL A/G bead slurry with 1 μg of the relevant antibody or IgG control. 650 μL of lysate was then incubated with antibody coated A/G beads for 2h rotating at 4°C. The remaining 50 μL of lysate was boiled with 10 μL 5X sample loading buffer with DTT. For non-reducing immunoprecipitations, DTT was omitted from sample loading buffer. After 2h, IP samples were centrifuged at 400 x g for 2min at 4°C, supernatant removed, and beads washed three times with 1mL low stringency lysis buffer. The immune complexes were eluted by addition of 50 μL 5X sample loading buffer, boiled for 5min (reducing) or heated at 50°C for 10min (non-reducing) and analyzed by SDS-PAGE.

RNA extraction and qPCR

Cell supernatant was removed, cells were washed with PBS and lysed in 350 μL lysis buffer (Ambion). The cell lysates were immediately frozen at −80°C and thawed gently prior to RNA extraction. Upon thawing, one volume 70% EtOH was added to allow for RNA

precipitation before transferring to Ambion RNA spin columns. The purification was followed as per manufacturer's instructions. The eluted RNA was quantified using a Nanodrop 2000 micro-volume UV-vis spectrophotometer and each RNA sample was diluted to the lowest yield before reverse-transcriptase PCR.

Disuccinimidyl suberate crosslinking

BMDMs were seeded at $1.5x10^6$ cells/mL in 6-well plates in technical duplicate and incubated at 37°C 5% CO_2 overnight. Cells were pre-treated with LPS (100ng/mL) for 3h. After 3h of LPS stimulation, media was removed and replaced with 1mL DMEM containing C1-27 for 45 min. After 45 min, cells were treated with ATP (5mM) for 45 min. Supernatant was removed and cells were washed twice with 200 μL ice cold HEPES (50mM). Cells were lysed on ice for 15min in 200 μL lysis solution (0.5% Triton X-100, 50mM HEPES, protease and phosphatase inhibitors). Duplicate samples were pooled and centrifuged at 6000 x g for 15 min at 4°C. The Triton X-100 soluble fraction (supernatant) was removed and stored at −20°C. The Triton X-100 insoluble fraction (pellet) was washed twice with HEPES (50mM) and centrifuged at 6000 x g for 15 min at 4°C. During the washing step, disuccinimidyl suberate-crosslinking buffer was made (50mM HEPES, 150mM NaCl pH 8). Disuccinimidyl suberate was allowed to reach RT prior to resuspension in anhydrous DMSO (54.3 μL DMSO to 2mg disuccinimidyl suberate for 100mM stock). The Triton X-100 insoluble pellet was resuspended in 490 μL disuccinimidyl suberate-crosslinking buffer and incubated with 10 μL rehydrated disuccinimidyl suberate (2mM final concentration), mixed immediately and incubated for 45min at 37°C. After 45min, samples were centrifuged at 6000 x g for 15 min at 4°C. The supernatant was removed gently, and the remaining disuccinimidyl suberate-crosslinked pellet was resuspended in 50 μL sample loading buffer containing DTT. Samples were analyzed by SDS-PAGE.

Confocal Microscopy

BMDMs were plated in 24-well plates at a density of $1x10^5$cells/mL on sterile 12mm cover glasses and left overnight at 37°C in 5% CO_2 incubator. Cells were primed with LPS (100ng/mL) for 3h, medium removed and treated with C1-27 for 45min. ATP (5mM) was added for 45min. Media was removed and cover glasses washed twice with PBS. Cells were fixed with 4% paraformaldehyde for 20min. Cover glasses were washed twice with PBS and permeabilized with 0.1% Triton X-100 for 25min. Cover glasses were washed twice with PBS and incubated with rabbit anti-ASC (1:100) overnight at 4°C. Cover glasses were washed with PBS for 20min and incubated with anti-rabbit Alexa Fluor 647 for 2h at RT. Cover glasses were washed twice with PBS for 20min, removed and mounted on 3 μL ProLong Gold antifade reagent with DAPI. Cover glasses were sealed with clear nail polish overnight at RT. A minimum of three images were taken from each sample for analysis. Images were acquired on a Leica SP8 scanning confocal microscope (Leica Microsystems) at x 20 magnification. For quantification of ASC speck positive cells, a minimum of 11 random regions of interest for each experimental condition were imaged and the number of ASC speck-positive cells were counted.

Colon organ culture

Colonic cytokine production was measured in supernatants from *ex vivo* organ culture. Distal colon segments (1 cm) were cut longitudinally and washed in ice cold PBS with penicillin (50 μg/mL), streptomycin sulfate (50 μg/mL), and neomycin sulfate (100 μg/mL) (Invitrogen). After washing, the wet weight of each sample was recorded. Each segment was cultured in 48-well culture plates with 350 μL serum-free RPMI-1640 medium supplemented with antibiotics for 24h in a humidified atmosphere of 5% CO_2 at 37°C. The supernatants were collected by centrifugation at 13,400 × g and 4°C for 3 min to remove tissue debris and then stored at −80°C until analyzed.

Histological Analysis

For histological analysis the colon was opened longitudinally and fixed in 10% buffered formalin. A roll of the organ was made to allow orientated histological assessment of the colon including the rectum. Following routine laboratory processing hematoxylin and eosin stained sections of the paraffin embedded tissues were prepared. The tissue was analyzed by a specialist Anatomical Pathologist (JED) in a blinded fashion. The criteria used for grading of inflammation have been previously described (Mladenova et al., 2011). Criteria used to grade inflammation included the presence of inflammatory cells in the mucosa and lamina propria, structural changes in the crypt architecture and expansion of the lamina propria.

Endogenous knockdown of GSTO1-1

BMDMs were seeded at $5x10^5$ cells/mL on 12-well plates and left overnight at 37°C in 5% CO_2 incubator. Cell medium was removed, and cells were washed briefly with PBS. 500 μL Opti-MEM reduced serum medium was added to cells. Scramble siRNA or GSTO1-1 siRNA was incubated with 5 μL RNAiMAX Lipofectamine reagent in 500 μL Opti-MEM for 10min. After incubation, 500 μL siRNA-lipofectamine mix was added to cells to yield 1mL of Opti-MEM medium containing 20nmol siRNA final concentration. Cells were left for 36h-48h before treatment.

NEK7 Expression and purification

The codon-optimized NEK7 gene construct was synthesized and cloned into $p^{J411KanR}$ (ATUM). The construct was overexpressed as an N-terminal His_6 tag fusion protein in *E. coli* BL21(DE3) (Novagen) at 18°C following induction with 0.5 mM IPTG. The cells were resuspended in sodium phosphate buffer (pH 7.0) (50 mM), NaCl (500 mM), 0.5% Triton X-100, β-ME (3 mM) and imidazole (Buffer

A) (30 mM) and lysed by French press (1500 psi). The lysate was cleared by centrifuging at 15000 rpm for 30 min and NEK7 was purified using a 5 mL HisTrap column (GE Healthcare) in Buffer A with up to 500 mM imidazole gradient. To cleave the His-tag, the eluted fractions were pooled and subjected to HRV3c protease digestion for overnight at 4°C in buffer A. The His-tag cleaved NEK7 was subsequently loaded and purified by passing through HisTrap column (GE Healthcare). The Ni-NTA purified NEK7 was dialysed into sodium phosphate buffer (pH 7.0) (50 mM), NaCl (150 mM) and further purified by the size exclusion chromatography (SEC) technique using a superdex 200 increase 10/300 gel filtration column (GE Healthcare). Similarly, GSTO1-1 wild-type and mutant proteins were expressed and purified as ubiquitin fusion proteins as previously described (Baker et al., 2005).

Surface plasmon resonance

Surface plasmon resonance (SPR) experiment was carried out at 25°C on a Biacore 8000 instrument (GE healthcare) using HBS buffer (10 mM HEPES-HCl, pH 7.4, and 150 mM NaCl) with EDTA (3 mM) and 0.05% P20 as a running buffer. The purified NEK7 was filtered and coupled (~1500 RU) onto CM5 sensor chip (GE healthcare) through amine coupling. The affinity measurement was performed by passing increasing concentrations of GSTO1-1 wild and mutant (up to 300 μM) at the flow rate of 5 μL/min. The final response unit was calculated by subtracting the response obtained from the reference flow cell. The data were fitted using the Biacore 8000 BIAevaluation software and GraphPad Prism Version 8.0 for data presentation.

Mass Spectrometry of NEK7

HEK293T cells were reverse transfected with HA-tagged NEK7. HEK293T cells were seeded at $7.5x10^5$ cells/mL in 10mL in 10cm dishes. During the plating, 10 μg NEK7 was transiently transfected into the HEK293T cells using GeneJuice and left overnight at 37°C in 5% CO_2 incubator. Cell medium was removed, cells were washed gently with PBS and cells were immediately lysed in low stringency lysis buffer containing protease and phosphatase inhibitors. An immunoprecipitation was performed using an anti-HA antibody conjugated to A/G beads. After 2h rotating at 4°C, A/G beads were washed three times with low stringency lysis buffer. After the third wash, the A/G beads were dried and incubated with 250 μL of 200 μg HA peptide or 30min at 37°C with gentle shaking. Beads were agitated every 5min to prevent sedimentation of A/G beads. A/G beads were centrifuged at 200 x g for 2min. Supernatant was removed and stored on ice. A/G beads were subsequently incubated with a further 250 μL of 200 μg HA peptide for 30min at 37°C at 300rpm and centrifuged at 400 x g for 2min. Both 250 μL supernatants were combined and concentrated using an Amicon Ultra 10K concentrating column (Merck Millipore). The concentrated eluate was incubated with GSSG (5mM, pH 8) for 1h at RT prior to loading on an 8% acrylamide gel. The 8% gel was fixed in Coomassie blue fixing solution (50% MeOH, 10% HoAC, 40% ultrapure H_2O) in a clear container for 30min on an orbital shaker at RT. Fixing solution was removed and replaced with Coomassie Blue R-250 for 1h at RT with gentle agitation. The gel was washed overnight at 4°C with de-staining solution (5% MeOH, 7.5% HoAC and 87.5% ultrapure H_2O). The gel bands were excised in a laminar flow hood and placed in sterile eppendorfs. 500 μL band wash solution was added (50% MeOH, 5% HoAC and 45% ultrapure H_2O) to eppendorfs and mixed at 1300rpm at RT for 2h, with wash solution changed every 30min to remove Coomassie stain. Gel bands were stored in 500 μL band wash solution on dry ice. Gel fragments were digested using Trypsin and analyzed by 1D nLC-MS/MS by a 4000QTRAP mass spectrometer. The resulting data was processed using the Mascot search engine with an ion cut score of 20.

NLRP3 Inflammasome Reconstitution in HEK293T cells

HEK293T cells were seeded at $2x10^5$ cells/mL in 24-well plates and left overnight at 37°C in 5% CO_2 incubator. The following morning, cells were transfected with plasmids encoding NLRP3 inflammasome components (ASC, 20ng; pro-IL-1β, 200ng; NLRP3, 200ng; pro-caspase-1; 100ng, and NEK7, 200ng; or NEK7 mutants, 200ng) and 200ng GSTO1-1 using Lipofectamine 2000. DNA concentration was kept constant by adding relevant EV control plasmid. Cells were left for 24h. After 24h, medium was replaced and supernatant was harvested 6h after medium change. Nigericin (10 μM) was added 1h prior to harvest. IL-1β secretion was analyzed by ELISA. This protocol was adapted from Shi et al. (2016a).

QUANTIFICATION AND STATISTICAL ANALYSIS

Statistical analysis

All statistical analyses were carried out using GraphPad Prism 8 (GraphPad Inc.) software. A Student's t test was used to compare two groups affected by a single variable, whereas a one-way ANOVA followed by Sidak's multiple comparisons test was used to compare multiple groups. Details of the statistical test used and the n number (representing biological replicates) can be found in the appropriate figure legend. All data are mean ± SEM. Differences were considered statistically significant at P values of *$p \leq 0.05$. ** signifies a P value of ≤ 0.01, *** signifies a P value of ≤ 0.001, and **** signifies a P value of < 0.0001.

DATA AND CODE AVAILABILITY

The published article contains all datasets generated or analyzed during this study.